Computational and Structural Biotechnology Journal 20 (2022) 675–684

COMPUTATIONAL AND STRUCTURAL BIOTECHNOLOGY JOURNAL

journal homepage: www.elsevier.com/locate/csbj

POT1-TPP1 binding stabilizes POT1, promoting efficient telomere maintenance

Tomas Aramburu, Joseph Kelich, Cory Rice, Emmanuel Skordalakes *

The Wistar Institute, 3601 Spruce St, Philadelphia, PA 19104, USA

ARTICLE INFO

Article history:
Received 18 October 2021
Received in revised form 7 January 2022
Accepted 7 January 2022
Available online 11 January 2022

Keywords:
Telomeres
POT1
TPP1
Cancer

ABSTRACT

Telomeric POT1-TPP1 binding is critical to telomere maintenance and disruption of this complex may lead to cancer. Current data suggests a reduction of intracellular POT1 levels in the absence of TPP1. Here we provide evidence of POT1 plasticity that contributes to its lack of stability in the absence of TPP1 binding. Structural data reveals inter- and intramolecular POT1C domain flexibility in the absence of TPP1. Thermostability and proteolytic resistance assays show that POT1C and the mutant complex POT1C(Q623H)-TPP1(PBD) are less stable than the wild type POT1C-TPP1(PBD), suggesting that TPP1 binding to POT1 stabilizes POT1C and makes it less accessible to proteasomal degradation in the cell. Disruption of the POT1-TPP1 complex such as through cancer-associated mutations leads to a reduction of intracellular POT1, telomere uncapping, and telomere associated DNA damage response (DDR). DDR in turn leads to senescence or genomic instability and oncogenesis.

1. Introduction

Telomeres are comprised of repeating nucleotide sequences and serve as protective caps at the ends of eukaryotic chromosomes. Replication of eukaryotic chromosomes leaves an uncopied overhang, resulting in gradual loss of genomic DNA and is known as the end replication problem [1]. Telomeres provide a solution to this problem by acting as a buffer between the chromosome ends and the transcribed portions of the genome [2,3]. Telomerase, a ribonucleoprotein reverse transcriptase, is responsible for elongating telomeres and increasing the replicative potential of certain cell types such as stem or cancer cells [4]. Telomerase dysregulation leads to chromosomal instability, age-related diseases and, in some instances, cancer [5,6].

POT1-TPP1, a subcomplex of shelterin, plays critical roles in telomere length regulation and maintenance. POT1 binds the telomeric overhang and suppress undesirable ATR-dependent DNA damage response (DDR) at telomeres. Misrecognition of telomeres by DDR pathways may result in conditions favorable for cancer such as chromosomal fusions and genomic instability [7,8]. The POT1-TPP1 complex also recruits telomerase to telomeres, enhancing its telomere replicative processivity [9,10]. The interaction of POT1 with TPP1 is beneficial for POT1 telomere localization as complex formation increases its ssDNA binding affinity highlighting the importance of POT1-TPP1 complex formation [9,10]. POT1-TPP1 binding is mediated by the POT1 C-terminal OB fold and the holiday junction resolvase domain (HJRD) while its N-terminal two OB folds engage single-stranded telomeric DNA (ssDNA) [10–14]. TPP1 consists of a N-terminal OB-fold and a POT1 and TIN2 binding domains (Fig. 1B) [14]. TPP1 localizes to telomeres via its interaction with TIN2 [15,16]while the N-terminal OB fold recruits telomerase to telomeres [17,18].

A recent study found that mutations disrupting the POT1-TPP1 complex resulted in reduced levels of POT1 in the cell [13], suggesting that POT1 is unstable in the absence of TPP1. Interestingly, cancer mutations found in triple-negative breast cancer occurring within the POT1-TPP1 binding interface similarly resulted in a drastic loss in intracellular POT1 [13]. These mutations likely contribute to cancer as they resulted in hallmarks of telomere uncapping with evidence of DDR, chromosomal fusions, and genomic instability [13]. To further understand the mechanism behind POT1 loss in the absence of POT1-TPP1 complex formation, we determined crystal structures of POT1C alone and screened for conformational differences compared to POT1-TPP1. Structural comparison of the TPP1-bound and TPP1-free POT1C revealed that the TPP1-free POT1C exhibits significant structural plasticity. Additionally, we performed thermostability assays including

* Corresponding author.
E-mail address: skorda@wistar.org (E. Skordalakes).

https://doi.org/10.1016/j.csbj.2022.01.005

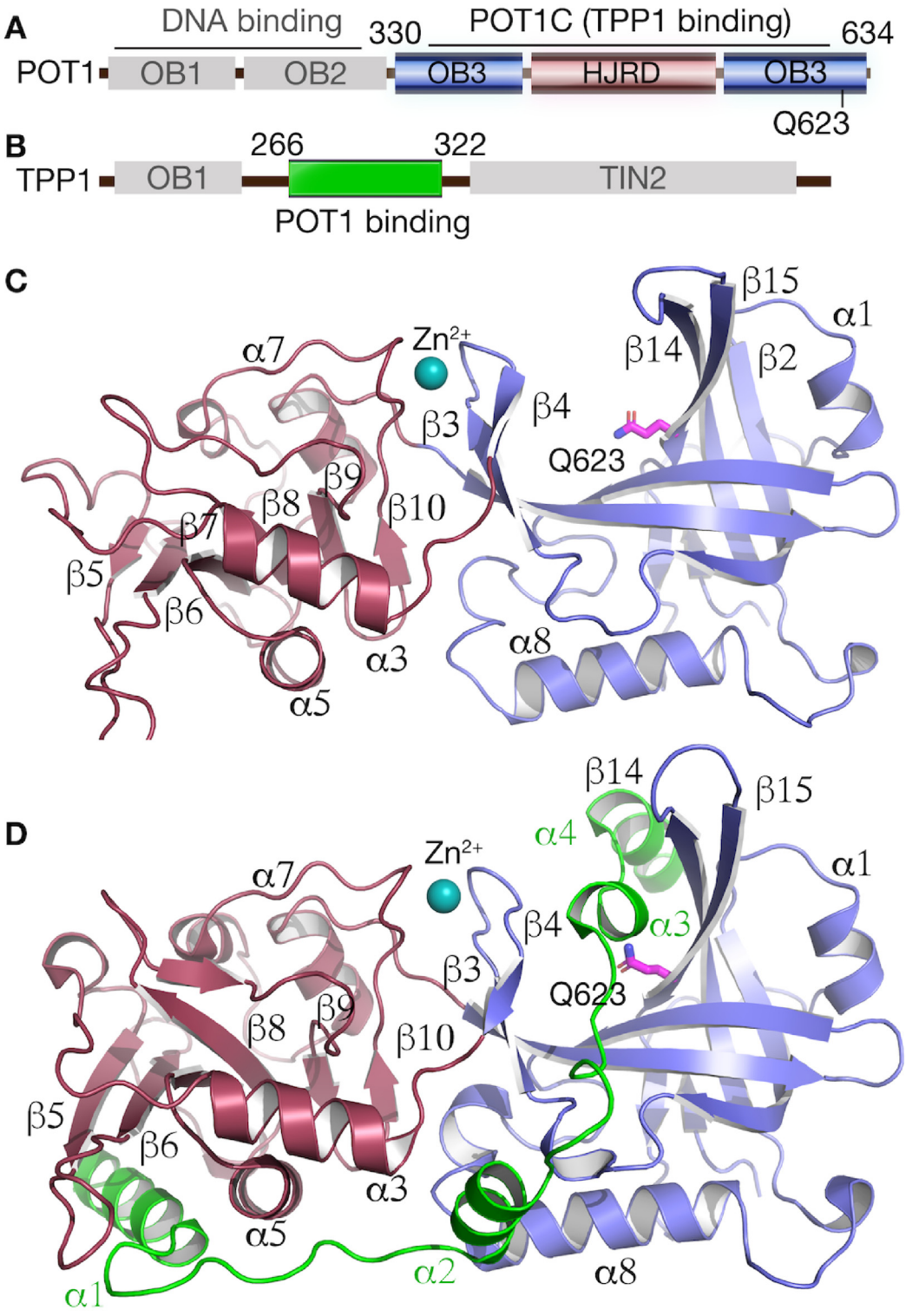

Fig. 1. Structures of POT1C and POT1C-TPP1(PBD). A & B. Primary structures of POT1 and TPP1. Domains and binding partners are indicated. C. POT1C monomer from CF1/2. The four-cysteine cluster (C382, C385, C503, C506) which coordinates a Zn^{2+} ion and stabilizes the two POT1 domains promoting the formation of an elongated bilobal structure, which provides an extensive surface area for TPP1 binding. D. Structure of POT1C-TPP1(PBD) from CF3, CF4 and CF5.

Differential Scanning Fluorimetry (DSF) [19], which also show that POT1 is thermolabile in the absence of TPP1. Finally, we show that consistent with the structural and thermostability assays, POT1C is more accessible to proteasomal degradation than the TTP1-bound form.

We propose that POT1 free of TPP1, resulting from mutations that affect complex formation is less structurally stable and more accessible to proteasomal degradation. This in turn leads to telomere uncapping, DDR, genomic instability, and cancer. These

findings provide novel evidence of the mechanism of action of cancer mutations that disrupt the POT1-TPP1 complex.

2. Results

2.1. Structure of POT1C

Here we report the crystal structures of POT1C, residues 330–634, from two distinct crystallization conditions with each generating a different crystal form. Crystals grown in 0.2 M DL-malic acid pH 7 and 30% PEG 600, which we will refer to as crystal form 1 (CF1), belong to the monoclinic space group $P2_1$ and contain two molecules in the asymmetric unit (AU). Crystals grown in 0.8 M ammonium phosphate pH 8.1, 24% PEG 4,000 and 7% 2-Methyl-2,4-pentanediol (MPD), which we will refer to as crystal form 2 (CF2), belong to the trigonal space group $P3_221$ and contain two molecules in the AU. The use of different crystal forms in this study is critical as it allows for the comparison of POT1C structures formed under distinct crystallization conditions and crystals forms thus providing several statistically significant independent measurements.

POT1C, as it has already been established from the published POT1C-TPP1(PBD) structure [13,14], is comprised of a classic OB-fold (OB; residues 330–390 and 539–634) and a holiday junction resolvase domain (HJRD; residues 391–538) (Fig. 1A). Notable structural features of the OB fold include a six-stranded β-sheet (β1-6) with a well-defined indentation on the surface of the protein forming part of the TPP1 binding pocket (Fig. 1C-D). The β-sheet is surrounded by two alpha helices (α1, 2). The HJRD is an insertion within the OB sequence and consists of seven anti-parallel beta-sheets (β7-13), surrounded by four alpha helices (α3-6). There is a four-cysteine cluster (C382, C385, C503, C506) at the interface of the OB-fold and the HJRD domain coordinating a Zn^{2+} ion, which stabilizes the extended conformation of the two domains.

Structural comparison of the CF1 and CF2 POT1C domains shows that the HJRD domain is highly flexible (RMSD: average 2.4 Å and max RMSD 14.9 Å) while the OB fold adopts overall a rigid conformation (RMSD: average 1.6 and max 7.2) (Fig. 2 and Movie 1). Domain differences are primarily associated with structural elements forming the TPP1-binding pockets of POT1C. These include helices α3 and α5 of the HJRD and the loop that connect strands β14 and β15 of the OB fold (Fig. 2). Significant differences are also observed for the surface loop that connects helix *a*3 to strand *b*5. This loop is not involved in TPP1 binding and is solvent accessible (Fig. 2A-E). These loops do not make any contacts in the crystal and therefore are free to adopt multiple conformations.

Interestingly, structural comparison of the four independent POT1C monomers CF1A/B and CF2A/B shows significant rigid domain motions, in addition to the intra-molecular differences observed primarily for the HJR domain. The POT1C rigid domain conformations arise from a hinge-like motion between its two domains, the HJRD and the OB fold (Fig. 2 and Movie 1). This motion allows the four POT1C monomers to adopt several conformations; one (CF1A) that we will refer to as "compact" as indicated by the solvent exposed surface area (15362 $Å^2$), and another that positions the two domains the furthest away from each other (CF2A - surface area 16447 $Å^2$), which we will refer to as the "loose" conformation. Within the "compact" and "loose" POT1C structures, we observe two intermediate conformational states. The presence of additional conformational states suggests a degree of interdomain flexibility within the "compact" and "loose" states. The structural diversity observed in CF1 and CF2 monomers is further supported by Differences Distance Matrix Program (DDMP [20]) structural analysis (Fig. 2F-K).

2.2. Structure of POT1C-TPP1(PBD)

In 2017 we and others published a structure of POT1C-TPP1 (PBD) (PDB ID: 5UN7 and 5H65) [13,14]. The TPP1 construct used in this study consists of residues 255–337 and the POT1 construct consists of residues 330–634 (Fig. 1A-B). Crystals of the tetragonal space group $P4_122$ grew from 2.4 M KCl, 50 mM K/Na Tartrate, 20 mM $BaCl_2$, and 0.1 M Sodium Citrate, pH 5.5. We will refer to this condition as crystal form 4 (CF4) and to the 5H65 structure/crystallization condition as CF5. During our attempt to crystallize the POT1-TPP1 complex, we tested different POT1-TPP1 constructs, including POT1 residues 325–634 and TPP1 245–327. Crystals of the monoclinic space group P1, grown from 0.1 M HEPES pH 7.5, and 3.0 M NaCl, contain four heterodimers in the asymmetric unit. We will refer to this condition as crystal form 3 (CF3). In 5UN7, the shorter TPP1 construct (residues 255–337) consists of 4 α-helices connected with extended loops. The longer construct of TPP1 used in this study adopts the same secondary/tertiary structure as in 5UN7 with the extra N-terminal residues 253–265 forming a helix (helix α0). Helix α0 does not make any contacts with POT1C, it is instead involved in crystal contacts with adjacent POT1C-TPP1 (PBD) heterodimers.

In CF3, CF4 and CF5, helix α1 of TPP1 interacts with a well-defined hydrophobic pocket of the HJRD, formed by the beta sheet (β5-7) and helices α3, α5 and the loops that connects them. Several conserved residues within this pocket (V434, W424, I455, V436, L453, F438, F470, C451, L445 and P446) make direct interactions with α1 L271, V272, A275, L279, L281 of TPP1 [14]. Helix α2 of TPP1 is located at the interface of the OB and HJRD. The large side chains of W293 and R297, that form part of helix α2 of TPP1, bind at the interface of the two OB3 and the HJRD further stabilizing the extended conformation adopted by POT1C. Helices α3 and α4 of TPP1 interact with the OB3 of POT1C. Residues Y306, M312, V308, L313, I315 and Y306 of TPP1 α3 interact with the canonical OB binding pocket residues V541, V543, M560, Y558, Q623, F625, Y610, C621 and P371 [14]. Helix α4 traverses the indentation formed by the β-barrel of the OB fold and interacts with the beta-strands β14 and β15 that form one of the walls of the OB binding pocket. Contacts between helix α4 of TPP1 involve residues D319, L323 of TPP1 and N611, P357, K608 and Q359 of POT1C [14]. Additional but limited contacts involve the coil regions of TPP1. Noteworthy are the interactions of Y306 and E303 of TPP1 with the side chains of P371and R372 and R373 of POT1C [14] respectively.

Structural comparison of CF4, CF5 with the four CF3 heterodimers shows that they are structurally similar (Fig. 3A-D). The RMSD between CF3A-D and CF4 heterodimers is 1.05 Å overall. Most of these differences are associated with solvent accessible loops of the HJRD (HJRD average RMSD = 0.95 Å; OB average RMSD = 0.55 Å) adopting multiple conformations. More specifically, the HJRD coil connecting α3 and β5 is displaced by a maximum of 5.5 Å between CF3 and CF4 (Fig. 3C). Additional subtle differences are observed at the tip of the TPP1 terminal helices α1 and α4 (Fig. 3C, D). These differences may result from the CF3 monomers having a longer TPP1 construct, which forms an additional helix (α0) involved in crystal contacts. The structural similarity observed in CF3 and CF4 monomers is further supported by DDMP structural analysis (Fig. 3E-M).

We have so far shown that POT1C is structurally flexible with the observed flexibility associated with intra- and intermolecular motions. We have also shown that POT1C is rigid when in complex with TPP1 adopting only a single conformation as confirmed by five distinct crystallographic measurements. Structural comparison of CF1/2(A-B) with CF3(A-D)/4/5 shows that the two POT1C domains, (the HJRD and the OB) undergo a rigid domain motion bringing the two domains closer by 3 Å when TPP1 binds (Fig. 4-

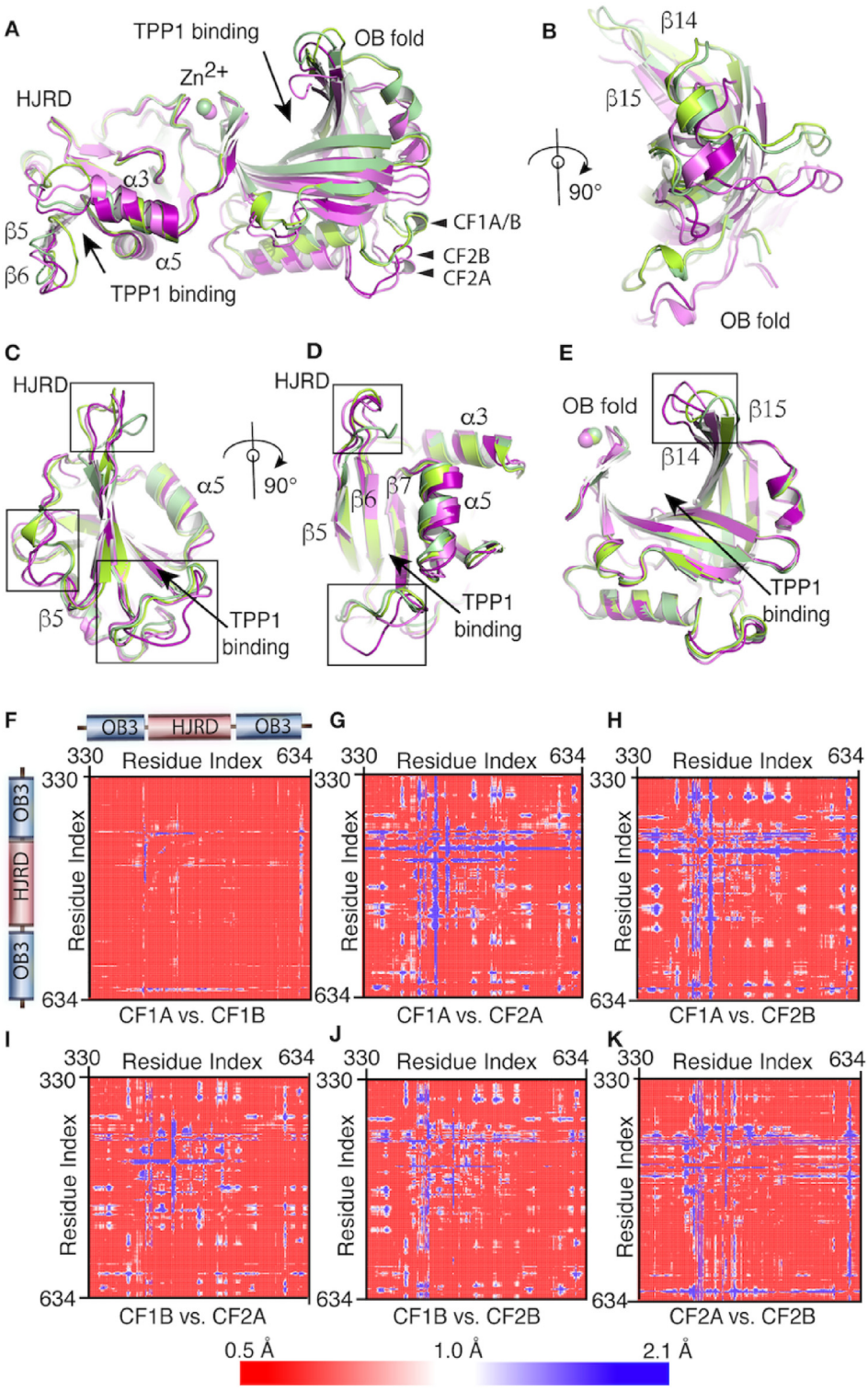

Fig. 2. Structural and DDMP comparison of the POT1C from two different crystal forms (CF1 and CF2). A. Overlay of CF1A (purple), CF1B (violet), CF2A (green) and CF2B (lime). Monomers are aligned to the HJRD. A hinge-like motion is observed between the OB fold and the HJRD of CF1/2A/B. B. 90° rotation of panel A shows a side view of the OB fold and illustrates the rigid domain differences between CF1A/B and CF2A/B. C. 90° rotation of panel B. Intradomain differences between the HJRD domains of the four monomers are shown. These include the loop connecting β5 to β6 and β6 to β7 and form part of the TPP1 binding pocket of POT1C. D. 90° rotation of panel C. E. Alignment of the OB fold shows that there are almost no intradomain motions, other than minor shifts along the solvent accessible loop connecting β14 and β15. F-K. DDMP comparison of the CF1A/B and CF2A/B POT1C monomers further supports the conformational flexibility of the POT1C structure. (For interpretation of the references to colour in this figure legend, the reader is referred to the web version of this article.)

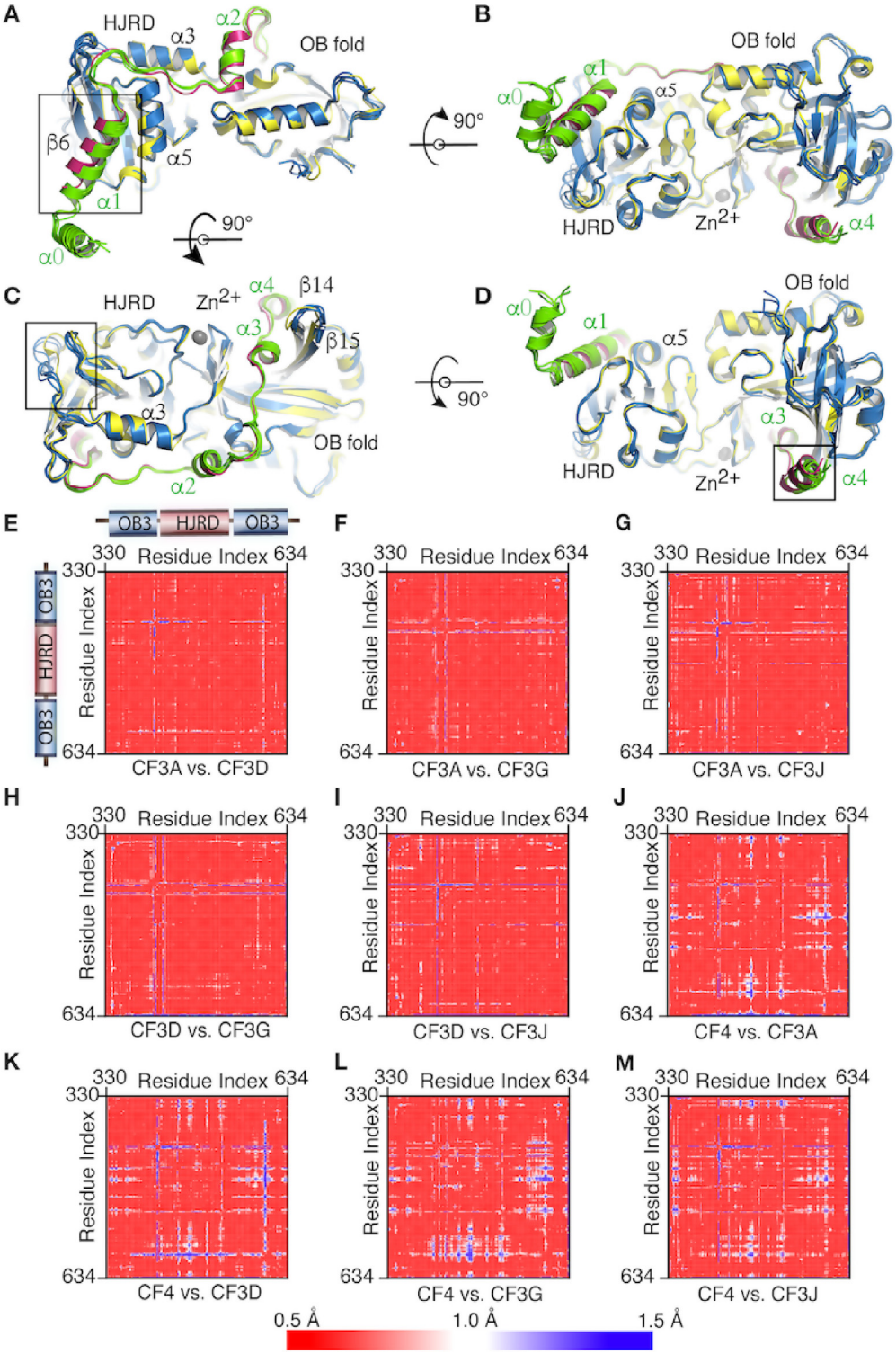

Fig. 3. Structural comparison of the five POT1C-TPP1(PBD) heterodimers from three distinct crystals forms (CF3, CF4 and CF5). A. Overlay of CF3A/B/C/D, CF4 and CF5 structures (POT1C – blue/yellow; TPP1 – green/red). B. 90° upward rotation of panel A. C. 90° downward rotation of panel A shows the canonical OB binding pocket. D. 90° downward rotation of panel C. E-M. DDMP comparison of the five independent POT1C monomers present in the CF3 and CF4 crystal forms shows the rigidity of POT1C when in complex with TPP1. (For interpretation of the references to colour in this figure legend, the reader is referred to the web version of this article.)

A-D). This domain motion arises from a 3 Å shift of the OB fold along the X axis and a 5° downward rotation along the Y axis. For CF2A/B and CF3/4 the domain rigid motion is even greater. The OB fold is shifted by 6 Å along the X axis and rotated 8° downwards along the Y axis. The changes in domain organization between the TPP1 bound and unbound POT1C structures are further reflected in the differences in their overall surface area and RMSD. While the CF1A/B monomers have an average surface area of 15,623 Å^2, the CF2/3/4 monomers have an average surface area of 16,400 Å^2.

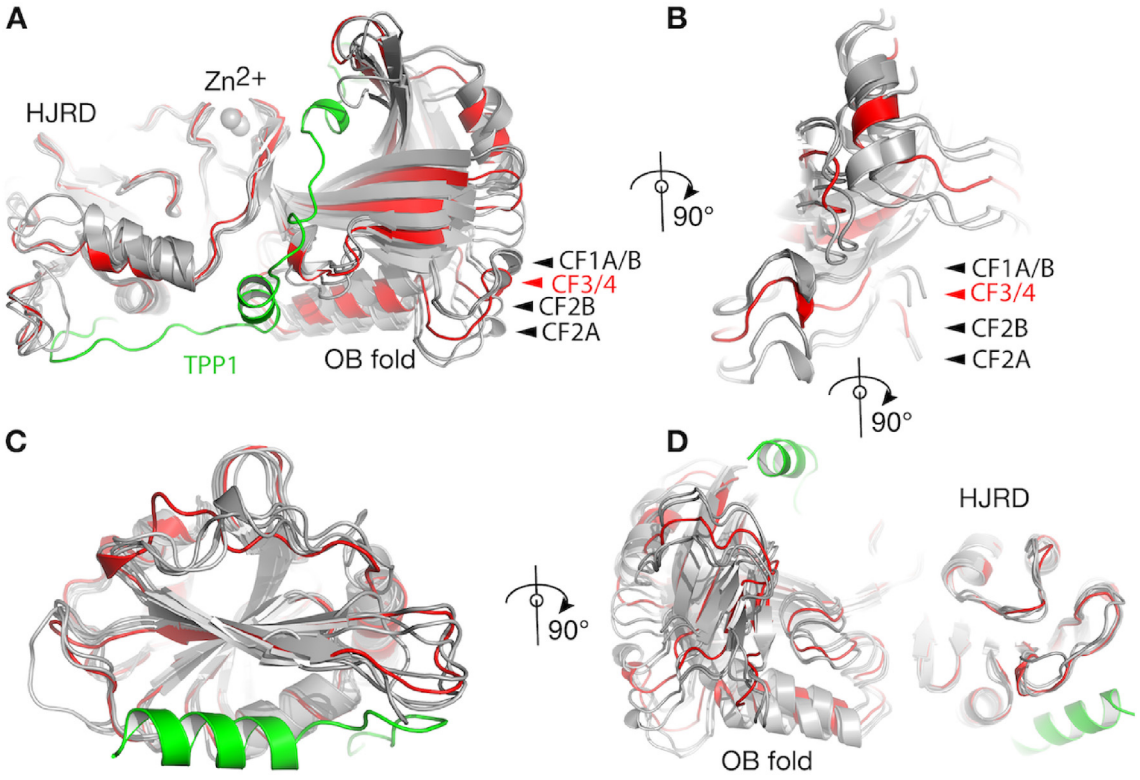

Fig. 4. Structural comparison of CF1/CF2 (TPP1 free) and CF3/CF4/CF5 (TPP1 bound). A. Structural comparison of CF1, CF2 (both colored grey), and CF4 (POT1 - red; TPP1 - green). Structures are aligned to the HJRD to illustrate the hinge-like motion between the two domains. B. 90° rotation of panel A. C. 90° of panel B. and D. 90° rotation of panel C. (For interpretation of the references to colour in this figure legend, the reader is referred to the web version of this article.)

2.3. POT1 is unstable in the absence of TPP1

To further examine POT1C plasticity, we performed B-factor analysis as well as thermostability and proteolytic stability assays of POT1C and POT1C-TPP1(PBD). B-factor analysis of the POT1C and POT1C-TPP1(PBD) structures show a high degree of thermal mobility for POT1C, especially for the HJR domain (Fig. 5A-C). We also carried out Differential Scanning Fluorimetry (DSF) experiments with purified POT1C, the cancer-associated mutant POT1C (Q623H)-TPP1(PBD) and the wild type POT1C-TPP1(PBD) as described previously [14]. We selected this cancer associated POT1 mutant protein because the residue Q623 is located on the surface of the protein and makes direct contacts with TPP1 (Fig. 1-C-D); it is not involved in the protein fold and therefore is ideal for this study. Based on previous studies from this lab, the POT1C (Q623H) mutant protein binds TPP1 with approximately 4–5 fold less affinity than the wild type POT1 [14]. The proteins were exposed to a temperature gradient of 20 – 95 °C using a qPCR thermocycler in the presence of SYPRO orange, which has an affinity for hydrophobic surfaces. The technique allows the detection of temperature-dependent protein denaturation by binding to exposed hydrophobic regions of the protein as it melts. The resulting melt curves revealed significant thermostability differences between POT1C, the mutant POT1C(Q623H)-TPP1(PBD) and the wild type POT1C-TPP1(PBD) (Fig. 5D). The apparent melting temperature (Tm °C) of POT1C, the mutant POT1C(Q623H)-TPP1 (PBD) and the wild type POT1C-TPP1(PBD) is 43.6 (SD = 0.46), 49.7 (SD = 0.25) and 56.3 (SD = 0.44) respectively. As expected, TPP1(PBD) alone, which only becomes structured upon POT1C binding, does not exhibit any significant SYPRO-associated signal. Each sample was run in six replicates.

We also performed proteolytic resistance assays using purified POT1C, the mutant POT1C(Q623H)-TPP1(PBD) and the wild type POT1C-TPP1(PBD) (Fig. 5E), and the human 26S proteasome (E-365, R&D systems). The proteins were incubated with the 26S proteasome at a 1(26S proteasome)/200(protein) ratio at room temperature overnight. The reactions were stopped by adding SDS PAGE loading dye and heating at 95 °C for 5 min. The results indicate that POT1C alone and the POT1C(Q623H)-TPP1(PBD) mutant complex are significantly more degraded than the wild type POT1C-TPP1(PBD) complex (Fig. 5E-F).

3. Discussion

While it has been shown that disruption of POT1-TPP1 binding in the cell leads to a loss of intracellular POT1 [13], the underlying cause has remained unclear. Here we reveal that POT1-TPP1 complex formation is essential for protein stability and thus intracellular abundance. In the absence of TPP1, POT1 exhibits significant structural plasticity, decreased thermostability, and rapid degradation by proteases. Loss of functional POT1 has been implicated in telomere uncapping and aberrant DNA damage response at telomeres. These conditions are favorable for genomic instability and cancer, highlighting the importance of POT1-TPP1 complex formation [21].

3.1. POT1C is structurally flexible adopting multiple interdomain conformations

The conformational dynamics associated with POT1-TPP1 binding have major implications for understanding proper POT1-TPP1 assembly and function. We found in the absence of TPP1(PBD), POT1C adopts a range of structural conformations indicating that it is a flexible protein with a certain freedom of conformational movement. Four POT1C independent measurements from two distinct crystal forms (CF1A/B and CF2A/B) show intradomain motions with an average RMSD of 2.4 Å and max RMSD 14.9 Å. Fur-

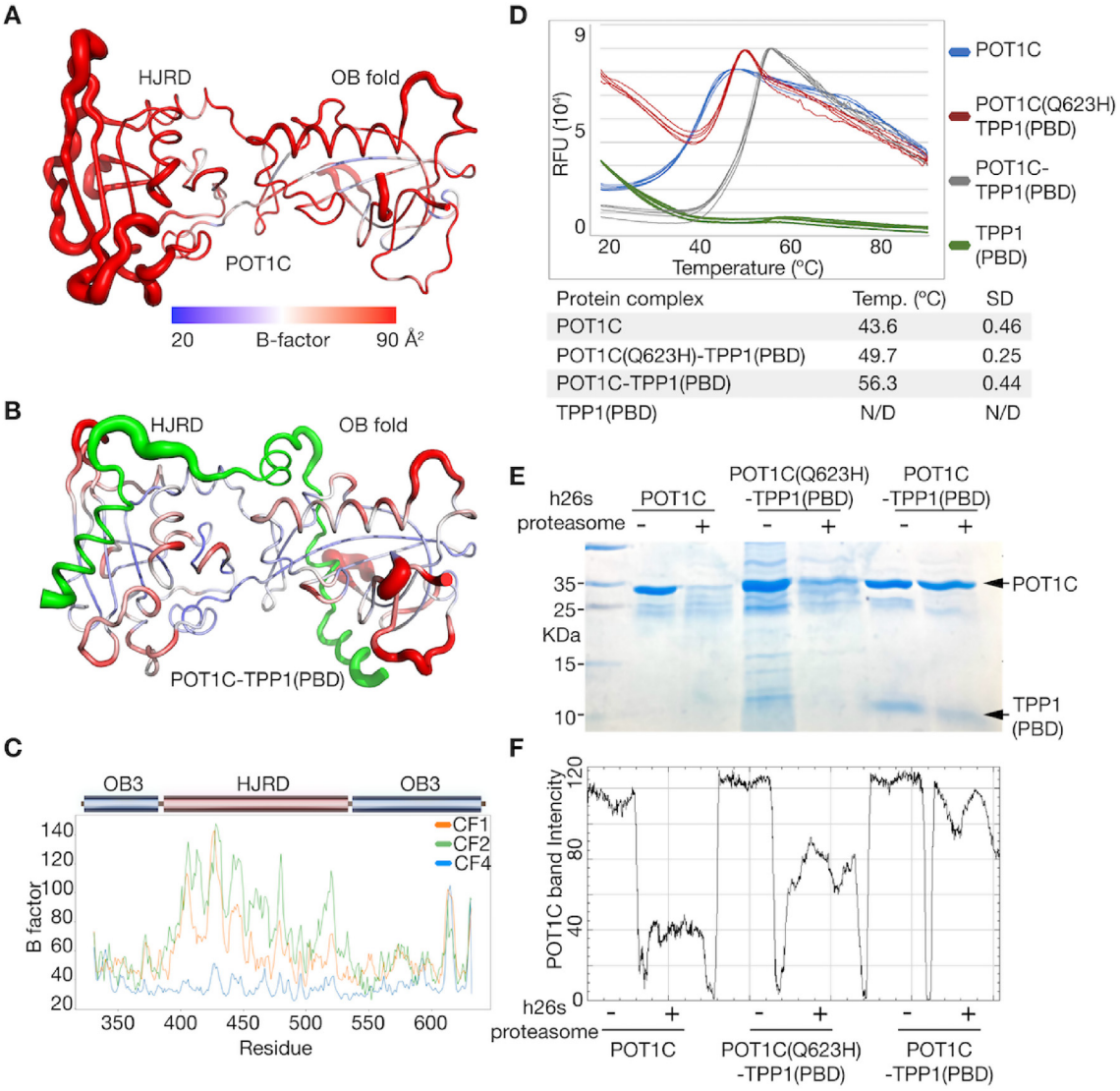

Protein complex	Temp. (°C)	SD
POT1C	43.6	0.46
POT1C(Q623H)-TPP1(PBD)	49.7	0.25
POT1C-TPP1(PBD)	56.3	0.44
TPP1(PBD)	N/D	N/D

Fig. 5. Structural stability of POT1C vs POT1C-TPP1(PBD). A, B & C. B factor analysis of the POT1C and POT1C-TPP1(PBD) structures. The analysis clearly shows that POT1C becomes rigid upon TPP1 complex formation. D. DSF assays of POT1C, POT1C(Q623H)-TPP1(PBD) cancer associated mutant and the wild type POT1C-TPP1(PBD) complex. The results indicate that the wild type POT1C-TPP1(PBD) complex has a much higher melting temperature than POT1C alone and the cancer mutant. E. Proteasomal degradation assays of POT1C, POT1C(Q623H)-TPP1(PBD) cancer associated mutant and the wild type POT1C-TPP1(PBD) complex. The data shows that POT1C and POT1C(Q623H)-TPP1 (PBD) are more susceptible to proteasomal degradation compared to wild type POT1C-TPP1(PBD). F. ImageJ [29] intensity plot of the POT1C bands from panel E.

ther evidence of the conformational changes and therefore plasticity of the POT1C monomer is reflected in the differences observed between the surface area of the four POT1C monomers ranging from 15362 Å^2 to 16447 Å^2.

The POT1C flexibility arises from intra- and interdomain motions. Of note, is the HJRD which shows flexibility throughout the domain while the conformational changes of the OB domain localize to the TPP1 binding pocket and in particular the loop that connects strands β14 and β15. HJRD intradomain motions include helices α3 and α5 , both of which form part of the TPP1 binding pocket. More specifically, α5 together with β5-7 bind helix α1 of TPP1. Helix α3 is in part located at the interface of the HJRD and the OB and makes contacts with helix α2 of TPP1. We observe that upon TPP1 binding helix α5 is shifted by 2 Å, toward the center of the HJRD TPP1 binding pocket forming a narrower channel that coordinates helix *a*1 of TPP1 (Fig. 4). Similarly, helix α3 of the HJRD pivots toward the OB fold contributing to the formation of a deep pocket at the interface of these domains allowing for the binding of the large side chains of W293 and R297 of TPP1 (Fig. 3 and 4).

3.2. The POT1C-TPP1 complex is rigid

In contrast to the flexible TPP1-free POT1C, the POT1C-TPP1 (PBD) complex adopts a rigid conformation (Fig. 3) as indicated by five independent structures (CF3A-D, CF4, and CF5). The average/maximum RMSD when comparing all five POT1C-TPP1(PBD) monomers is ~ 1.05 Å. The OB fold maximum RMSD between all five heterodimers is 0.55 Å, while that while of the HJRD is 0.95 Å. The inflated RMSD between the CF3A-D and CF4 structures is due to subtle differences between them resulting from a) the CF3A-D structures having a longer TPP1 construct and b) the flexibility of solvent accessible loops not involved in crystal contacts. The longer TPP1 construct contains an additional N-terminal helix (α0) involved in crystal contacts. Furthermore, the solvent accessible surface area of these structures ranges from 16250 Å^2 to 16429 Å^2, amounting to less than 1% difference across the five POT1C-TPP1(PBD) heterodimers. The low RMSD and conserved solvent accessible area between CF3 and CF4 further supports our hypothesis that the POT1C-TPP1 complex is rigid.

3.3. TPP1 samples and binds the most favorable POT1C structural conformation

So far, we have established that POT1C is structurally flexible while the TPP1-bound POT1C is structurally rigid. Structural comparison of CF1/CF2 and CF3/CF4 structures show intra- and interdomain conformational differences for the TPP1-free, POT1C structure. Intradomain conformational changes are observed primarily for the TPP1 binding pocket of the HJRD of POT1C (Fig. 2). Helices α3 and α5 located on the surface of POT1C form part of a largely hydrophobic pocket that accommodates helix α1 of TPP1 (Fig. 4). Helix α3 shifts roughly 1.7 Å and helix α5 moves approximately 2 Å toward the center of the TPP1 binding pocket. The shift allows for the formation of a tight hydrophobic pocket that binds the TPP1 helix α1 making extensive interactions with this leucine rich structural element. Intradomain conformational changes are also observed for the OB fold but those are limited to the β14 and β15 and the loop that connects them (Fig. 2). It is worth noting that these two strands form part of the OB fold's TPP1 binding pocket.

A striking difference between the CF1/CF2 and CF3/CF4 structures is a rigid domain motion between the OB fold and the HJRD (Fig. 4). Superposition of the HJRD of CF1, CF2 and CF3/4/5, places each of the OB fold in distinct positions from one another in the 3D space (Fig. 4). Interestingly, CF3/4/5 is most closely related to the CF2 monomers with an average RMSD of 1.4 Å when compared to CF3/4/5. The same value for CF2B is 1 Å. In contrast the RMSD for CF1A and CF1B when compared to CF3/4/5 is 1.8 Å and 1.6 Å respectively. The data suggests that the CF2A/B monomer is more closely related to the CF3/4 conformation although not the same, suggesting that POT1C can adopt a range of interdomain conformations including the one observed in the TPP1 bound state (CF3/4/5). TPP1 samples all these interdomain conformations of POT1C and binds the most favorable one stabilizing this conformation and increasing its frequency in solution.

3.4. Disruption of POT1-TPP1 interactions may drive cancer

POT1 mutations have been implicated in a form of breast cancer lacking expression of estrogen receptor, progesterone receptor and HER2 called triple-negative breast cancer [21,22]. The triple-negative breast cancer-associated POT1 mutations P371T within the TPP1 interacting region of POT1 was shown to result in a drastic reduction of intracellular protein levels when expressed ectopically compared to wild type POT1 [13]. The POT1 Q623H mutation present in glioma and melanoma [23], which was biochemically shown to result in partial inhibition of POT1-TPP1 complex formation, was found to be similarly unstable compared to wild type POT1 [13,14]. Moreover, co-expression of wild type POT1 with TPP1 lacking the POT1-binding domain (PBD), resulted in significant lower levels of wild type POT1 [13]. All three mutations resulted in deprotected telomeres, DDR, increased chromosomal fusions and genomic instability providing evidence that defects in POT1-TPP1 interactions potentially drive cancer. Our DSF experiments show that POT1C as well as the mutant POT1C(Q623H)-TPP1(PBD) are strikingly less stable in solution, with their melting temperature ∼ 13 and 6 °C less than that of the POT1C-TPP1(PBD) complex respectively. We also show through proteolytic resistance assays that POT1C and the mutant POT1C(Q623H)-TPP1(PBD) are significantly more accessible to proteolytic degradation, by the human 26S proteasome, compared to the wild type POT1C-TPP1 (PBD) complex. Taking these data together, we propose that the decrease of intracellular POT1 upon loss of TPP1 binding is due to POT1 protein stability issues followed by increased accessibility to proteasomal degradation. This mechanism bears some similarities to other clinically relevant protein–protein interactions which stabilize proteins. Transmembrane channel-like protein 1 (TMC1) is a critical component of the mechanotransduction complex of the inner ear [24]. This protein is stabilized upon binding of another protein named LHFPL5. When this complex is disrupted through mutation, TMC1 expression was drastically reduced. The loss of this complex formation may contribute to deafness [24]. A similar situation has been reported for the oncogene protein p73 which becomes more stable in response to binding MDM2. MDM2 binding is believed to prevent proteasomal degradation and increase intracellular levels of p73 [25]. The loss of POT1 stability occurring from cancer-associated mutations, such as POT1 (Q623H), disrupting POT1-TPP1 complex formation result in less net available POT1 for capping telomeres. This loss of telomere protection may contribute to cancer development.

4. Materials and methods

4.1. Protein expression and purification

The C-terminus of human POT1 (residues 330–634) was cloned into a pET28b vector with a 6xHis-pMocr fusion tag, cleavable by TEV protease. POT1C was overexpressed in *E. coli* ScarabXpress T7 *lac* competent (Scarab Genomics) at 16 °C for 18 h, following induction by 1 mM IPTG (isopropyl-β-D-thiogalactopyranoside; Gold Biotechnology). The cells were harvested by centrifugation (4,500 rpm, 20 min, 4 °C) and lysed by sonication in a buffer containing 95% Ni.NTA Buffer A (25 mM Tris-HCl pH 7.5, 1.0 M KCl, 1.0 M urea, 5% glycerol, 1.0 mM phenylmethylsulfonyl fluoride (PMSF), and 1.0 mM benzamidine) and 5% Ni.NTA Buffer B (25 mM Tris-HCl pH 7.5, 150 mM KCl, 300 mM imidazole, 5% glycerol, 1.0 mM PMSF, and 1.0 mM benzamidine). Protein lysate was centrifuged at 18,000 rpm (20 min, 4°. C) and the supernatant was loaded onto a Ni-nitrilotriacetic acid (NiNTA - MCLab) column. Buffer was exchanged on the column to Ni.NTA Buffer C (25 mM Tris-HCl pH 7.5, 150 mM KCl, 5% glycerol) and the protein was eluted with Ni.NTA Buffer B directly onto tandem HS (poros) – HQ (poros) columns equilibrated with Ni.NTA Buffer C. POT1C was eluted from the HQ column with a gradient from 0.15 M KCl to 1.0 M KCl. The pMocr tag was cleaved overnight at 4° C with TEV protease. Cleaved POT1C was again run through tandem HS-HQ columns equilibrated with 0.2 M KCl. Size exclusion chromatography (Superdex S200, GE Healthcare) with Dialysis Buffer (10 mM Tris-HCl pH 7.5, 100 mM KCl, 1 mM TCEP) was used to remove any remaining impurities and aggregates. We prepared two TPP1 constructs, one consisted of residues 255–337 the other of residues 245–337. The human POT1C-TPP1 (PBD) protein complex (CF4) was prepared as described in Rice et al [14].

4.2. Protein crystallization

Protein was concentrated to 10 mg/mL and dialyzed into a buffer containing 10 mM Tris-HCl pH 7.5, 100 mM KCl, and 1 mM TCEP. POT1C crystallized at room temperature under two sitting-drop vapor diffusion conditions. Crystal form 1 (CF1) contained 200 mM DL-Malic acid pH 7.0, 30% v./v. polyethylene glycol (PEG) 600 with the addition of 6% methanol. Crystal form 2 (CF2) contained 800 mM ammonium phosphate pH 8.1, 24% w./v. PEG 4,000 with the addition of 7% 2-Methyl-2,4-pentanediol.

The POT1C-TPP1 (PBD) heterodimer also crystallized under two sitting-drop vapor diffusion conditions at room temperature. The POT1C-TPP1 (PBD) complex with the longer TPP1 construct (residues 245–337) crystallized under a condition containing 0.1 M HEPES pH 7.5 and 3.0 M NaCl (CF3). The condition for crystal form 4 (CF4) is described by Rice et al [14].

Table 1
Data collection and refinement statistics for POT1C Structures.

POT1	CF1A/B	CF2A/B	CF3
Data collection			
Space group	$P2_1$	$P3_221$	P1
Cell dimensions			
a, *b*, *c* (Å), *β* (°)	61.98 61.80 83.74 94.493	162.59 162.59 63.57	70.88 70.98 103.79 76.764 84.613 70.549
Resolution (Å)	20–2.55 (2.62–2.55)*	20–2.65 (2.72–2.65)	20–2.9 (2.81–2.90)*
CC(1/2)	99.7 (49.5)	99.9 (53.4)	99.5 (41.2)
I / s*I*	13.9 (1.2)	20.9 (2.0)	8.9 (0.9)
Completeness (%)	98.3 (82.3)	99.4 (95.7)	89.66 (85.2)
Redundancy	7.2 (5.2)	10.8 (9.7)	5.9 (5.5)
Refinement			
Resolution (Å)	20–2.55	20–2.65	20–2.90
No. of reflections	21,455	28,208	36,811
R_{work} / R_{free}	22.6/28.2	19.2/20.0	26.5/28.7
No. atoms			
Protein	4860	4860	11,812
Ligand/ion	2	2	4
Water	75	70	34
Mean B value	49	50	55
R.m.s. deviations			
Bond lengths (Å)	0.003	0.011	0.024
Bond angles (°)	0.687	1.307	2.027
Ramachandran Plot			
Favored	95.17	87.17	90.05
Allowed	4.83	12.83	9.14
Outliers	0.0	0.0	0.81

*Values in parentheses are for highest-resolution shell.

5. Data collection and structure determination

Data for CF1 and CF2 were collected in house on a Rigaku MicroMax-007 HF rotating anode X-ray generator (wavelength 1. 54178 Å) with VariMax optics and using a Saturn 944 HG CCD detector. The crystals were flush frozen in liq. N_2 and were kept frozen with an Oxford Cryosystems Cobra system at 100° K during the data collection. CF1 crystals diffracted to 2.55 Å resolution, belong to the monoclinic space group ($P2_1$), and contain 2 monomers in the asymmetric unit (AU) (Table 1). CF2 crystals diffracted to 2.65 Å resolution, belong to the trigonal space group ($P3_221$), and contain 2 monomers in the AU (Table 1). The data was processed and scaled with XDS [26]. The POT1-TPP1 (CF3) crystals were collected at 1.008 Å wavelength at BL12-2 SSRL. CF3 crystals diffracted to 2.9 Å resolution, belong to the P1 space group, and contain 4 monomers in the AU (Table 1). The CF1 and CF2 structures were solved by molecular replacement using the 5UN7 model in phenix [27] after removing the TPP1 coordinates. The CF3 structure was solved using the 5UN7 model in phenix. The structures were refined in phenix and models were build when necessary in Coot [28]. For CF4 crystals see Rice et al [14]. The coordinates and structure factors for the CF1, CF2 and CF3 structures have been deposited in the RCSB database and the relevant PDB ID numbers are 7S1O 7S1U and 7S1T respectively.

5.1. DDMP

For the DDMP calculations, the distance between pairs of the Cα atoms in one molecule is measured and tabulated in matrix form. The same is done for the second molecule. The matrices are subtracted from one another to yield the difference in relative displacement of Cα atoms, which is the difference distance matrix. Difference distance matrix plots were produce using the DDMP program from the Center for Structural Biology at Yale University, New Haven, CT.

5.2. Differential Scanning Fluorimetry

We further tested the thermostability of the POT1C, TPP1, POT1C-TPP1 (PBD), and POT1C (Q623H)-TPP1 (PBD) proteins using a 7500 Fast Real-Time thermocycler(Thermo Fischer). The proteins were diluted in a buffer consisting of 20 mM HEPES at pH 7.5, 0.15 M KCl, 5% glycerol and 1 mM TCEP to a final concentration of 10uM and heated from 20 to 95 °C at a scan rate of 60 °C per hour. The thermogram for each protein sample was normalized to the buffer and data analysis was performed using DSFworld (https://bio.tools/dsfworld).

5.3. Proteolysis

Purified POT1C (residues 330–632), the mutant POT1C(Q623H)-TPP1(PBD) and the wild type POT1C-TPP1(PBD) and resuspended at a final concentration of ~10 uM in a buffer consisting of 20 mM Hepes, 150 mM KCl, 5% glycerol, 1 mM ATP, 5 mM $MgCl_2$, 1 mM TCEP, pH 7.2. The proteins were incubated at room temperature with the human 26S proteasome at a ratio of 200 (protein) to 1 (proteasome) overnight. The reactions were stopped by adding SDS gel loading dye and incubating at 95 °C for 5 mins prior to running on a 12% SDS page gel.

Declaration of Competing Interest

The authors declare that they have no known competing financial interests or personal relationships that could have appeared to influence the work reported in this paper.

Acknowledgements

The research was funded by the NCI (1 RO1 CA201312-01) and The Wistar Cancer Center Support Grant (P30 CA10815).

Appendix A. Supplementary data

Supplementary data to this article can be found online at https://doi.org/10.1016/j.csbj.2022.01.005.

References

[1] de Lange T. How telomeres solve the end-protection problem. Science 2009;326(5955):948–52.
[2] Cech TR, Lingner J. Telomerase and the chromosome end replication problem. Ciba Found Symp 1997;211:20–8. discussion 28–34.
[3] Lingner J, Cooper JP, Cech TR. Telomerase and DNA end replication: no longer a lagging strand problem? Science 1995;269(5230):1533–4.
[4] Shampay J, Blackburn EH. Generation of telomere-length heterogeneity in Saccharomyces cerevisiae. Proc Natl Acad Sci 1988;85(2):534–8.
[5] Bernardes de Jesus B, Blasco MA. Telomerase at the intersection of cancer and aging. Trends Genet 2013;29(9):513–20.
[6] Carneiro MC, de Castro IP, Ferreira MG. Telomeres in aging and disease: lessons from zebrafish. Dis Model Mech 2016;9(7):737–48.
[7] Denchi EL, de Lange T. Protection of telomeres through independent control of ATM and ATR by TRF2 and POT1. Nature 2007;448(7157):1068–71.
[8] Tong A, Stern JL, Sfeir A, Kartawinata M, de Lange T, Zhu X-D, et al. ATM and ATR Signaling Regulate the Recruitment of Human Telomerase to Telomeres. Cell Rep 2015;13(8):1633–46.
[9] Wang F, Podell ER, Zaug AJ, Yang Y, Baciu P, Cech TR, et al. The POT1-TPP1 telomere complex is a telomerase processivity factor. Nature 2007;445 (7127):506–10.
[10] Nandakumar J, Cech TR. DNA-induced dimerization of the single-stranded DNA binding telomeric protein Pot1 from Schizosaccharomyces pombe. Nucleic Acids Res 2012;40(1):235–44.
[11] Lei M, Podell ER, Cech TR. Structure of human POT1 bound to telomeric single-stranded DNA provides a model for chromosome end-protection. Nat Struct Mol Biol 2004;11(12):1223–9.
[12] Loayza D, Parsons H, Donigian J, Hoke K, de Lange T. DNA binding features of human POT1: a nonamer 5'-TAGGGTTAG-3' minimal binding site, sequence specificity, and internal binding to multimeric sites. J Biol Chem 2004;279 (13):13241–8.
[13] Chen C et al. Structural insights into POT1-TPP1 interaction and POT1 C-terminal mutations in human cancer. Nat Commun 2017;8:14929.
[14] Rice C et al. Structural and functional analysis of the human POT1-TPP1 telomeric complex. Nat Commun 2017;8:14928.
[15] Hu C, Rai R, Huang C, Broton C, Long J, Xu Y, et al. Structural and functional analyses of the mammalian TIN2-TPP1-TRF2 telomeric complex. Cell Res 2017;27(12):1485–502.
[16] Takai KK, Kibe T, Donigian JR, Frescas D, de Lange T. Telomere Protection by TPP1/POT1 Requires Tethering to TIN2. Mol Cell 2017;67(1):162. https://doi.org/10.1016/j.molcel.2017.05.033.
[17] Nandakumar J, Bell CF, Weidenfeld I, Zaug AJ, Leinwand LA, Cech TR. The TEL patch of telomere protein TPP1 mediates telomerase recruitment and processivity. Nature 2012;492(7428):285–9.
[18] Tejera AM, Stagno d'Alcontres M, Thanasoula M, Marion RM, Martinez P, Liao C, et al. TPP1 is required for TERT recruitment, telomere elongation during nuclear reprogramming, and normal skin development in mice. Dev Cell 2010;18(5):775–89.
[19] Niesen FH, Berglund H, Vedadi M. The use of differential scanning fluorimetry to detect ligand interactions that promote protein stability. Nat Protoc 2007;2 (9):2212–21.
[20] Richards FM, Kundrot CE. Identification of structural motifs from protein coordinate data: secondary structure and first-level supersecondary structure. Proteins 1988;3(2):71–84.
[21] Wu Y, Poulos RC, Reddel RR. Role of POT1 in human cancer. Cancers 2020;12 (10):2739.
[22] Foulkes WD, Smith IE, Reis-Filho JS. Triple-negative breast cancer. N Engl J Med 2010;363(20):1938–48.
[23] Shi J, Yang XR, Ballew B, Rotunno M, Calista D, Fargnoli MC, et al. Rare missense variants in POT1 predispose to familial cutaneous malignant melanoma. Nat Genet 2014;46(5):482–6.
[24] Yu X, Zhao Q, Li X, Chen Y, Tian Ye, Liu S, et al. Deafness mutation D572N of TMC1 destabilizes TMC1 expression by disrupting LHFPL5 binding. Proc Natl Acad Sci 2020;117(47):29894–903.
[25] Ongkeko WM, Wang XQ, Siu WY, Lau AWS, Yamashita K, Harris AL, et al. MDM2 and MDMX bind and stabilize the p53-related protein p73. Curr Biol 1999;9(15):829–32.
[26] Kabsch W. Integration, scaling, space-group assignment and post-refinement. Acta Crystallogr D Biol Crystallogr 2010;66(2):133–44.
[27] Adams PD, Afonine PV, Bunkóczi G, Chen VB, Davis IW, Echols N, et al. PHENIX: a comprehensive Python-based system for macromolecular structure solution. Acta Crystallogr D Biol Crystallogr 2010;66(2):213–21.
[28] Emsley P, Cowtan K. Coot: model-building tools for molecular graphics. Acta Crystallogr D Biol Crystallogr 2004;60(12):2126–32.
[29] Schneider CA, Rasband WS, Eliceiri KW. NIH Image to ImageJ: 25 years of image analysis. Nat Methods 2012;9(7):671–5.